

Average [O II] nebular emission associated with Mg II absorbers: Dependence on Fe II absorption

Ravi Joshi^{1*}, Raghunathan Srianand², Patrick Petitjean³ and Pasquier Noterdaeme³

¹*Kavli Institute for Astronomy and Astrophysics, Peking University, Beijing 100871, China*

²*Inter-University Centre for Astronomy and Astrophysics, Post Bag 4, Ganeshkhind, Pune 411007, India*

³*UPMC-CNRS, UMR7095, Institut d'Astrophysique de Paris, F-75014 Paris, France*

Accepted —. Received —; in original form —

ABSTRACT

We investigate the effect of Fe II equivalent width (W_{2600}) and fibre size on the average luminosity of [O II] $\lambda\lambda 3727, 3729$ nebular emission associated with Mg II absorbers (at $0.55 \leq z \leq 1.3$) in the composite spectra of quasars obtained with 3 and 2 arcsec fibres in the Sloan Digital Sky Survey. We confirm the presence of strong correlations between [O II] luminosity ($L_{[\text{O II}]}$) and equivalent width (W_{2796}) and redshift of Mg II absorbers. However, we show $L_{[\text{O II}]}$ and average luminosity surface density suffers from fibre size effects. More importantly, for a given fibre size the average $L_{[\text{O II}]}$ strongly depends on the equivalent width of Fe II absorption lines and found to be higher for Mg II absorbers with $\mathcal{R} \equiv W_{2600}/W_{2796} \geq 0.5$. In fact, we show the observed strong correlations of $L_{[\text{O II}]}$ with W_{2796} and z of Mg II absorbers are mainly driven by such systems. Direct [O II] detections also confirm the link between $L_{[\text{O II}]}$ and \mathcal{R} . Therefore, one has to pay attention to the fibre losses and dependence of redshift evolution of Mg II absorbers on W_{2600} before using them as a luminosity unbiased probe of global star formation rate density. We show that the [O II] nebular emission detected in the stacked spectrum is not dominated by few direct detections (i.e., detections $\geq 3\sigma$ significant level). On an average the systems with $\mathcal{R} \geq 0.5$ and $W_{2796} \geq 2\text{\AA}$ are more reddened, showing colour excess $E(B - V) \sim 0.02$, with respect to the systems with $\mathcal{R} < 0.5$ and most likely traces the high H I column density systems.

Key words: galaxies: evolution, galaxies: ISM, quasars: absorption lines, galaxies: star formation, cosmology: observations

1 INTRODUCTION

Understanding the surface star-formation rate (Σ_{SFR}) and its redshift dependence associated with quasar absorbers is of utmost importance for measuring the star-formation rate density (SFRD) as a function of cosmic time in a luminosity independent way (Wolfe et al. 2003; Srianand et al. 2005; Rahmani et al. 2010; Ménard et al. 2011) and to probe the Kennicutt-Schmidt law in low metallicity gas at high redshifts (Rahmani et al. 2010). Evidence for large scale outflows are seen in nearly all star-forming galaxies in the local Universe and out to $z \sim 6$ (Pettini et al. 2001; Shapley et al. 2003; Steidel et al. 2010; Martin et al. 2012; Newman et al. 2012; Lundgren et al. 2012; Zhu et al. 2015). Wind detection rates in galaxies at intermediate and low redshifts are found to be depending on the galaxy orientation with the

outflow geometry being consistent with a bi-conical flow (Martin et al. 2012). These winds are thought to be responsible for enriching the intergalactic medium (IGM) and circumgalactic medium (CGM) around galaxies (Schaye 2001; Simcoe et al. 2012). At high redshifts, for isolated galaxies, gas inflowing rate is found to be roughly comparable to the sum of the star formation rate and the outflowing rate (Erb 2008; Seko et al. 2016).

At present, the best way to probe the low density outflowing gas is to study the metal absorption lines they imprint in the spectra of background luminous sources (at small impact parameters; $\rho < 10$ kpc) which trace the dynamic environment, i.e., gas inflows and outflows in the outskirts of galaxies over cosmic time-line (Weisheit 1978; Lanzetta & Bowen 1992; Mo & Miralda-Escude 1996; Tinker & Chen 2008; Chelouche & Bowen 2010; Bouché et al. 2012). In the local Universe winds are ubiquitous in galaxies having Σ_{SFR}

* E-mail: rvjoshirv@gmail.com(RJ)

$\geq 0.1 M_{\odot} \text{ yr}^{-1} \text{ kpc}^{-2}$ (Heckman 2001, 2002). If high Mg II equivalent width systems are associated with outflows, as suggested by Nestor et al. (2011) and Bouché et al. (2012), then the associated galaxy is expected to have high Σ_{SFR} . Therefore, understanding the connection between absorber properties and their associated galaxies (e.g., equivalent width vs Σ_{SFR}) is vital for understanding various feedback processes that shape up the galaxy evolution.

Interestingly, the average Σ_{SFR} per absorber can be obtained using spectral stacking exercise (Wild et al. 2007; Noterdaeme et al. 2010; Ménard et al. 2011) by making suitable assumptions related to fibre losses. Note that, in spectroscopic surveys using fibres (e.g., 3 and 2 arcsec fibres used in SDSS-DR7 and DR12 surveys) one not only integrate light from the background quasar but also from all foreground galaxies that happen to fall within the fibre. However, because of various practical reasons it is highly probable that only a part of the line emitting region of foreground galaxy may come inside the fibre and this leads to the fibre loss. This loss will also have redshift dependence. At low redshifts $0.4 < z < 1.3$, in a stacking experiment of 3461 Mg II and 345 Ca II absorbers, Wild et al. (2007) have detected the [O II] nebular emission and measured an average star formation rate (SFR) of $0.11 - 0.14 M_{\odot} \text{ yr}^{-1}$ and $0.11 - 0.48 M_{\odot} \text{ yr}^{-1}$, respectively. Using the enlarged sample of Mg II absorbers from SDSS-DR7, Noterdaeme et al. (2010) have detected the average [O II] luminosity of $\sim 1.4 - 5.1 \times 10^{40} \text{ erg s}^{-1}$ for strong Mg II absorbers (i.e., $W_{2796} \geq 1 \text{ \AA}$) at $0.5 < z < 0.7$. Ménard et al. (2011) proposed that Mg II absorbers recover the overall star formation history of the universe and can be used as a new tool to probe the redshift evolution of SFR in a luminosity independent manner. Rahmani et al. (2010) have stacked the damped-Ly α absorbers (DLA) with $\log N(\text{H I}) \geq 20.3$ to detect the average Ly α emission and set an upper limit on the contribution of DLA galaxies to the cosmic SFRD of $\sim 0.13 M_{\odot} \text{ yr}^{-1} \text{ Mpc}^{-3}$ at $z \sim 3$ (see also, Noterdaeme et al. 2014; Joshi et al. 2017a). However, as mentioned above physical parameters derived from fibre spectra suffer from effect of fibre losses and one has to be mindful of this while interpreting these results (López & Chen 2012; Joshi et al. 2017b).

Fibre losses can in principle be considered as negligible for systems with large W_{2796} because of the well known anticorrelation between impact parameter (ρ) and W_{2796} (Bergeron 1986; Steidel 1995; Chen et al. 2010; Nielsen et al. 2013). López & Chen (2012) have shown that for the fibre size used in SDSS-II (3 arcsec), galaxies associated with more than 90% of the systems will fall inside the fibre for $W_{2796} > 3 \text{ \AA}$ (see their figure 4). However, large scatter in W_{2796} vs ρ relationship could increase the fibre loss. A strong correlation is seen between the Mg II equivalent width (at low spectral resolution is a good proxy to the velocity spread along the line of sight) and galaxy color where a stronger Mg II absorbers tend to be present in the vicinity of star-forming galaxies and most likely to be associated with the outflows (Zibetti et al. 2007; Noterdaeme et al. 2010; Bordoloi et al. 2011; Lan et al. 2014; Nielsen et al. 2016). The absorbing gas traced by Mg II absorbers appear to have a bimodality in azimuthal angle distribution where the cool dense gas is preferred to lie near major and minor axes of galaxies (Bouché et al. 2012; Kacprzak et al. 2012).

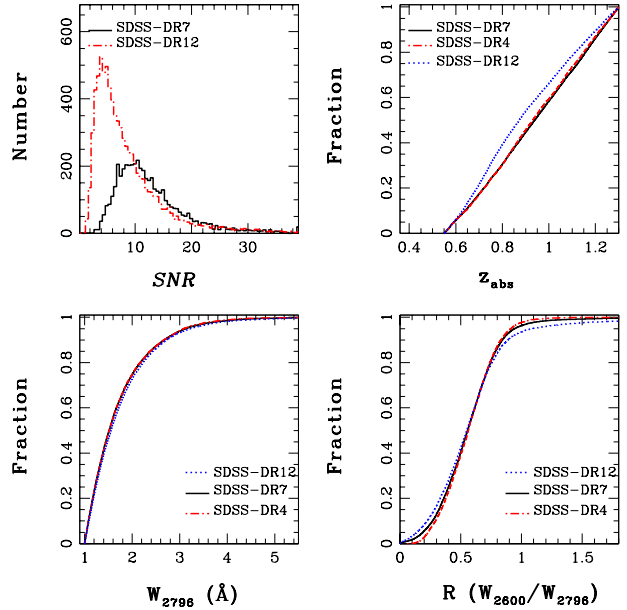


Figure 1. *Top left panel:* The signal-to-noise ratio distribution of quasar spectra around the expected position of [O II] emission line in SDSS-DR7 and DR12 spectra. The cumulative distribution of the z_{abs} (*top right*) and $\mathcal{R} \equiv W_{2600}/W_{2796}$ (*bottom right*) of our Mg II systems from SDSS-DR7 and SDSS-DR4 Mg II systems used in Ménard et al. (2011).

The Mg II absorbers with strong Fe II absorption are likely to arise from either very high metallicity sub-DLAs or high $N(\text{H I})$ DLAs (Srianand 1996; Rao et al. 2006). Rao et al. (2006) have found that the detection rate of DLAs in Mg II systems increases if one puts additional constraints based on equivalent width ratios of Mg II, Mg I and Fe II absorption. They detected DLAs with a success rate of ~ 42 per cent by selecting Mg II absorbers with strong Fe II absorption (i.e., $\mathcal{R} \equiv W_{2600}/W_{2796} \geq 0.5$) and $W_{2852} > 0.1 \text{ \AA}$. In recent efforts to detect cold gas in strong Mg II systems Dutta et al. (2017) have found a factor four times higher detection rate of H I 21-cm absorption in systems with $W_{2600} \geq 1 \text{ \AA}$ (see also, Gupta et al. 2012). Recently, we have detected 198 [O II] emitting galaxies associated with strong Mg II absorbers in the spectra of SDSS (Joshi et al. 2017b, hereinafter refer as Paper 1). We have found that the Mg II absorbers detected in [O II] nebular emission (with $L_{[\text{O II}]} > 2 \times 10^{40} \text{ erg s}^{-1}$) typically have $W_{2796} \geq 1 \text{ \AA}$, Mg II doublet ratio ($DR = W_{\text{Mg II}\lambda 2796}/W_{\text{Mg II}\lambda 2803}$) close to unity and $\mathcal{R} \geq 0.5$. Therefore, given the above facts, naively one would expect a strong dependence of average [O II] luminosity of Mg II absorbers in the stacked spectra of systems with different \mathcal{R} parameter ranges.

There are two main motivations behind this work: (i) to study the dependence of average $L_{[\text{O II}]}$ on \mathcal{R} and (ii) to understand the effect of fibre size on different observed correlations between $L_{[\text{O II}]}$ and other parameters. While the former allows us to probe the nature of SFR in potential DLA candidates the latter will allow us to probe the gas distribution at different scale around the star forming regions probed by different samples of Mg II absorbers.

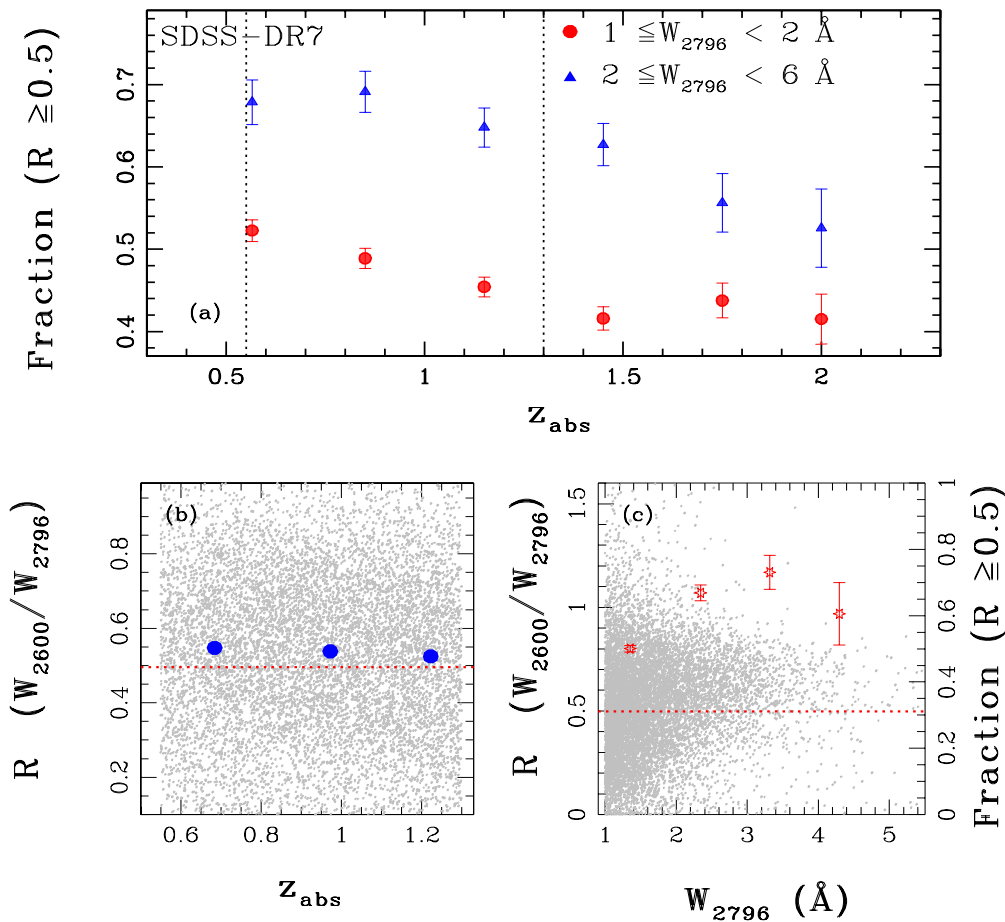


Figure 2. *Top panel:* The fraction of Mg II systems with $R \geq 0.5$ versus z for two different W_{2796} ranges. Vertical dotted lines mark the redshift range of interest for this study. *Bottom right panel:* The dependence of \mathcal{R} parameter on W_{2796} for the Mg II systems. The corresponding fraction is shown as stars in the right side ordinate. For this plot we consider only Mg II systems in the redshift range of our interest. *Bottom left panel:* \mathcal{R} as a function of redshift for systems with $W_{2796} \geq 1 \text{ \AA}$. The solid blue circles show the median value of \mathcal{R} in different redshift bins. The results are for Mg II systems from SDSS-DR7 (see Fig A1 in Appendix A1 for the results based on SDSS-DR12).

This article is organized as follows. Section 2 describes our sample of absorbers used in this study. In Section 3, we present the spectral stacking analysis. In Section 4, we present various correlations seen in the stacked spectra of quasars from SDSS-DR7 and DR12. Here, we also discuss the dependence of [O II] on \mathcal{R} parameter. Finally, discussions and conclusions are presented in Section 5. Throughout, we have assumed a flat cosmology with $H_0 = 70 \text{ km s}^{-1} \text{ Mpc}^{-1}$, $\Omega_m = 0.3$ and $\Omega_\Lambda = 0.7$.

2 SAMPLE

We have constructed a sample of strong Mg II absorbers, defined as the ones with rest equivalent width $W_{2796} \geq 1 \text{ \AA}$ (detected at $\geq 4\sigma$), by using the compilation of Mg II systems from the *expanded-version* of JHU-SDSS Metal Absorption Line Catalog¹ (Zhu & Ménard 2013), compiled from the SDSS-DR7 and SDSS-DR12. For a fully saturated line

this equivalent width threshold corresponds to a velocity spread of $\sim 107 \text{ km s}^{-1}$. We select only systems with velocity offset of $> 5000 \text{ km s}^{-1}$ with respect to the quasar emission redshift and avoid sightlines having broad absorption lines produced by quasar outflows (i.e., BALQSOs). To investigate the dependence of the average [O II] luminosity in the stacked spectra on \mathcal{R} parameter we ensured that the Fe II $\lambda 2600$ line falls in the wavelength range of higher completeness at $\lambda > 4000 \text{ \AA}$, i.e., $z \geq 0.55$ and redward of Ly α emission of the quasar. In addition, we restrict ourselves to $z \leq 1.3$ (i.e. $\lambda \lesssim 8500 \text{ \AA}$ for [O II] $\lambda 3727, 3729$ line) to avoid the [O II] emission being contaminated by most crowded telluric lines. For the above redshift range, i.e., $0.55 \leq z \leq 1.3$, the fibres of 3 and 2 arcsec diameter used for the SDSS-DR7 and DR12 observations project an angular size of $\sim 9.6 - 12.5 \text{ kpc}$ and $\sim 6.4 - 8.4 \text{ kpc}$, respectively, in the sky. Our final sample consists of 10,083 and 12,116 Mg II systems from SDSS-DR7 and DR12, respectively.

We note that our sample of Mg II systems based on SDSS-DR7 is similar to the SDSS-DR4 sample used by

¹ <http://www.pha.jhu.edu/~gz323/Site/>

Ménard et al. (2011) in terms of z_{abs} , W_{2796} and $\mathcal{R} \equiv W_{2600}/W_{2796}$ (see also, Fig. 1). A two-sided Kolmogorov-Smirnov test (KS-test) finds no difference between the two sub-samples based on z_{abs} , W_{2796} and \mathcal{R} parameters with a null probability of being drawn from the same parent distribution to be $P_{KS} = 0.8$, 0.8 and 0.7 , respectively. The median redshift probed in SDSS-DR7 and DR4 sample is $z_{\text{abs}} \sim 0.9$. However, SDSS-DR7 has twice the number of Mg II systems in the sample of Ménard et al. (2011). The Mg II systems detected in SDSS-DR12 also show a similar W_{2796} distribution as seen in SDSS-DR7 and DR4. However, the absorption redshifts (z_{abs}) of Mg II systems in SDSS-DR12 are found to be slightly lower with a median $z_{\text{abs}} \sim 0.8$. One can note that the average SNR , measured around the expected [O II] nebular emission, for the SDSS-DR7 spectra is slightly higher than the SDSS-DR12 spectra (top left panel in Fig. 1). The mean (respectively, median) \mathcal{R} parameter of Mg II systems from SDSS-DR4, DR7 and DR12 is found to be ~ 0.57 (0.56), ~ 0.56 (0.56), ~ 0.55 (0.54), respectively.

In panel (a) of Fig. 2 we show the evolution of fraction of strong Mg II absorbers with $\mathcal{R} \geq 0.5$ as a function of redshift. It is clear from the figure that over the redshift range of our interest (i.e. $0.55 \leq z \leq 1.3$ identified with vertical dotted lines in Fig. 2) the fraction of absorbers with $\mathcal{R} \geq 0.5$ in the range $1 \text{ \AA} \leq W_{2796} < 2 \text{ \AA}$ decreases from 53% to 44%. However, this fraction remains nearly constant at $\sim 70\%$ for the systems with $2 \text{ \AA} \leq W_{2796} \leq 6 \text{ \AA}$ over the same redshift range (i.e., region between the two dotted lines in Fig. 2). Even these strong systems show decreasing trend when we consider the full observed z range.

Dey et al. (2015) have found the median \mathcal{R} values to decrease with increasing z for Mg II systems detected in SDSS-DR7. We see the same trend with Mg II systems detected in SDSS-DR12 for the full sample (see Fig. A1 in Appendix A1). Based on their fit (see their figure 2) we expect \mathcal{R} to decrease by 0.04 between redshift 0.5 and 1.3. For systems in the restricted redshift range of our interest (i.e., $0.55 \leq z \leq 1.3$) we do see a similar evolution of \mathcal{R} with redshift where \mathcal{R} decreases by ~ 0.03 (see panel b of Fig. 2). They interpreted this evolution to be due to evolution in the metallicity ratio [Fe/Mg], most probably caused by the cosmic evolution in the SNIa rates. In panel (c) of Fig. 2 we plot \mathcal{R} as a function of W_{2796} for all the systems in the z range of our interest. The dependence of \mathcal{R} on W_{2796} is apparent as the fraction of systems with $\mathcal{R} \geq 0.5$ increases from $\sim 50\%$ to $\sim 80\%$ for the W_{2796} range from 1 \AA to 3 \AA .

3 ANALYSIS

To detect the [O II] nebular emission from Mg II absorbers we have constructed composite spectra, using continuum subtracted spectra and median statistics. For this, we have shifted the individual spectrum to the rest-frame of the Mg II absorber by conserving the flux and rebinning on to a uniform rest wavelength grid as the original data (Bolton et al. 2012). We modeled the local continuum by a low order (typically a third order) polynomial fit, within the proximity of [O II] $\lambda\lambda 3727, 3729$ line (i.e., rest wavelength range of $3700 - 3750 \text{ \AA}$). While stacking, we have masked the absorption line features originating from systems at

other redshifts as well as the sky emission lines in the spectrum. The 1σ flux uncertainty in each pixel in the stacked spectrum is estimated from the central interval encompassing 68% of the flux distribution of the corresponding pixel as in Joshi et al. (2017a).

Recall that the physical area corresponding to a given angular aperture varies with redshift. As suggested by Ménard et al. (2011), to account for the fibre effects, we also generate the stacked spectrum of [O II] luminosity surface density ($\Sigma_{[\text{O II}]}$). To estimate the $\Sigma_{[\text{O II}]}$, we convert each spectrum into luminosity units, at the redshift of the absorber and divide by the projected surface area of the fibre at the absorber redshift before co-adding them to get the composite spectrum that we will call $\Sigma_{[\text{O II}]}$.

As expected we detect [O II] emission in most of our composite spectra. In each composite spectrum we model the observed [O II] emission line with a double Gaussian profile with a tied linewidth but freely varying the line ratio in a range of 3.4-1.5², allowing for the typical range in the electron density of the gas under photoionization equilibrium. Gaussian fitting is mainly used to verify any possible dependences of intensity ratio of [O II] doublet and its FWHM with Mg II absorption line properties. However, we simply integrate the stacked spectrum over the central 12 pixels (i.e., $\sim 800 \text{ km s}^{-1}$) for measuring the [O II] line luminosity (or $\Sigma_{[\text{O II}]}$) and the respective error is computed by propagating the flux uncertainty in each pixel.

We have also generated geometric mean composite spectra to study the effect of \mathcal{R} parameter on the average reddening induced by Mg II absorbers (York et al. 2006; Khare et al. 2012). For this, we have shifted each spectrum to the absorber rest frame and computed their geometric mean. Here, we do not use the normalized or continuum subtracted spectrum to preserve the average continuum shape which is important for determining the characteristic extinction law (see also, York et al. 2006). To compute the relative extinction we have generated the stacked spectra for a control sample of quasars, within $\Delta z = \pm 0.05$ of z_{em} and $\Delta r_{\text{mag}} = \pm 0.5$ of r_{mag} , without absorbers in their spectra. We will discuss the results of this analysis in Section 4.5.

4 RESULTS

We generate several composite spectra in various W_{2796} and redshift bins. Since, we are interested in measuring the average [O II] nebular emission line luminosity (or surface brightness) associated with the Mg II absorbers, the direct detection of [O II] nebular emission reported in Paper 1 are also included in most of our analysis. We also present the results when these systems are excluded from the analysis.

4.1 Average [O II] emission and fibre effects

To quantify the fibre loss effect we have constructed composite spectra by dividing our sample into five W_{2796} bins

² The [O II] $\lambda 3729/\lambda 3727$ intensity ratio in the range 3.4-1.5 is predicted in photoionization models for the electron density in the range $n_e = 10^1 - 10^5 \text{ cm}^{-3}$ for the kinetic temperature $T = 10,000 \text{ K}$ (Osterbrock & Ferland 2006).

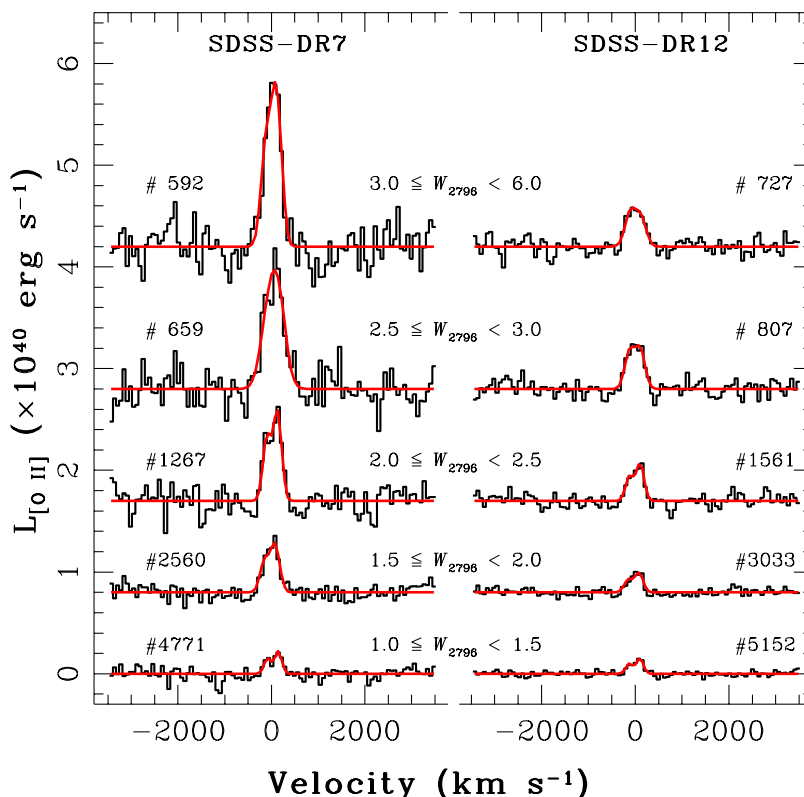


Figure 3. The [O II] emission line profile seen in SDSS-DR7 (*left*) and DR12 (*right*) stacked spectra for various W_{2796} bins. The *solid* line shows the best fit double Gaussian to the data. The continuum-subtracted spectra are shifted by a constant offset in luminosity for display purpose.

of $1 - 1.5$, $1.5 - 2.0$, $2.0 - 2.5$, $2.5 - 3.0$ and $\geq 3 \text{ \AA}$ for SDSS-DR7 and DR12. The stacked profiles for various W_{2796} bins and the number of systems used to construct the stacked spectra are shown in Fig. 3. It is apparent that for a given equivalent width bin the [O II] line luminosity found for SDSS-DR7 is higher than that of SDSS-DR12. In the *left panel* of Fig. 4, we show the median [O II] line luminosity as a function of W_{2796} for the Mg II systems in SDSS-DR7 (*circles*) and DR12 (*triangles*). We find a clear increasing trend of $L_{[\text{O II}]}$ with increasing W_{2796} . This is consistent with the trend found by Noterdaeme et al. (2010) in a stacking analysis of Mg II systems they have found from SDSS-DR7 quasars. We note that median $L_{[\text{O II}]}$ we detect in SDSS-DR7 sample is similar to that obtained by Noterdaeme et al. (2010, see also their table 5).

In *right panel* of Fig. 4, we show $\Sigma_{[\text{O II}]}$ as a function of W_{2796} . We confirm the strong correlation between W_{2796} and $\Sigma_{[\text{O II}]}$ in both the SDSS-DR7 (*circles*) and DR12 (*triangles*) datasets. The $\Sigma_{[\text{O II}]}$ measurement for SDSS-DR7 and DR12 datasets for each W_{2796} bin are listed in column 4 and 7 of Table 1, respectively. We first compare our results based on SDSS-DR7 stacked spectra with that of Menard et al. (2011), based on SDSS-DR4, as spectra were obtained using 3 arcsec fibre in both cases. Note that our redshift range of $0.55 \leq z \leq 1.3$ is slightly different from that of Menard et al.

(2011) of $0.36 \leq z \leq 1.3$. As suggested by Menard et al. (2011) we model this relationship using a powerlaw of the form $\langle \Sigma_{[\text{O II}]} \rangle = AW_0^\alpha$ and compute the best fit parameters of $\alpha = 1.69 \pm 0.11$ and $A = (2.55 \pm 0.27) \times 10^{37} \text{ erg s}^{-1} \text{ kpc}^{-2}$ for SDSS-DR7. While comparing our best fit parameters with Menard et al. (2011), i.e., $\alpha = 1.75 \pm 0.11$ and $A = (1.48 \pm 0.18) \times 10^{37} \text{ erg s}^{-1} \text{ kpc}^{-2}$, the α is found to be same whereas normalization factor is found to be different (i.e. ~ 1.7 times higher) at a significance level of $\sim 3.3\sigma$. We note that this difference in the normalization factor is mainly due to difference in the way quasar continuum is modelled. Menard et al. (2011) have modelled the continuum with an iterative running median of sizes ranging from 500 to 15 pixels. This basically smooths all small scale fluctuations. In fact, we get the similar values of $\Sigma_{[\text{O II}]}$ if we use the continuum fitting procedure adopted by Menard et al. (2011) [see Fig. A2 and related discussions in the Appendix]. However, for rest of the paper we will present result from data using our continuum fitting procedure.

It is clear from the figure that $\Sigma_{[\text{O II}]}$ measured from the SDSS-DR7 data are higher than those from SDSS-DR12 data (apart from the first equivalent width bin). The difference in 3 out of the 5 equivalent width bin considered here is more than 2σ (see column 4 and 7 of Table 1). The best fitted relationship between $\Sigma_{[\text{O II}]}$ and W_{2796} for the SDSS-DR12

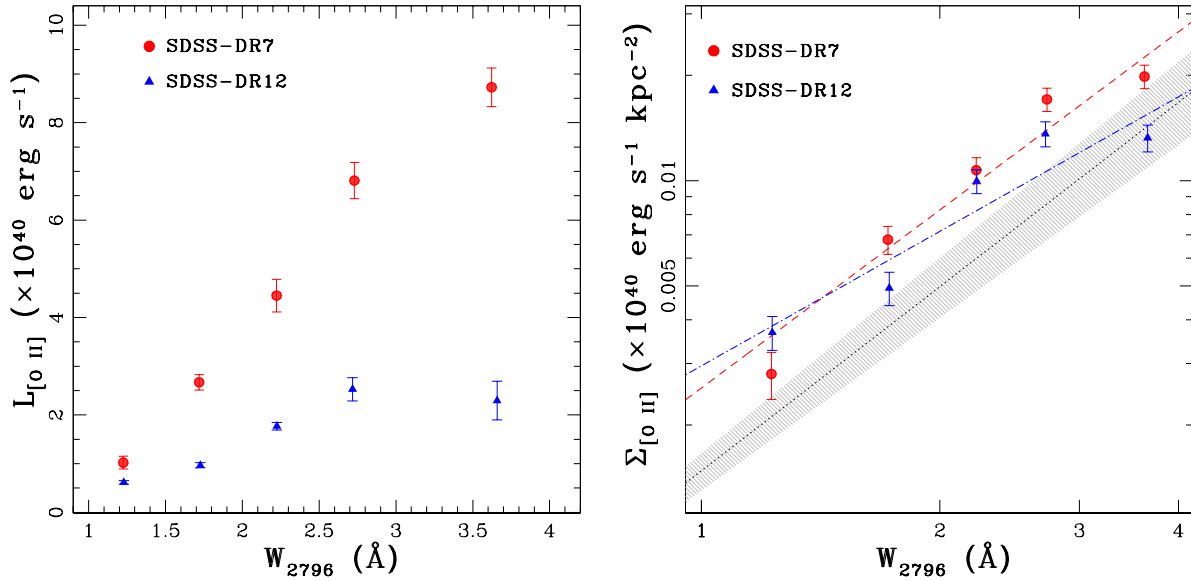


Figure 4. *Left panel:* The [O II] luminosity of Mg II absorbers for various W_{2796} bins for SDSS-DR7 (red circles) and DR12 (blue triangles). *Right panel:* The [O II] luminosity surface density ($\Sigma_{[\text{O II}]}$) as a function of W_{2796} for SDSS-DR7 (red circles) and DR12 (blue triangles). The dotted line shows the best fit for $\Sigma_{[\text{O II}]}$ versus W_{2796} from Ménard et al. (2011) while shaded region show the 1σ uncertainty (see Appendix A2 for more discussion on this difference). The dashed and dot-dashed line are the best-fitting power law for our measurements based on SDSS-DR7 and DR12 data set.

Table 1. [O II] luminosity surface density traced by Mg II absorbers as a function of equivalent width (W_{2796}).

W_{2796} interval (Å)	$\Sigma_{[\text{O II}]}$ for SDSS-DR7			$\Sigma_{[\text{O II}]}$ for SDSS-DR12		
	$\langle W_{2796} \rangle$ (Å)	$\langle z \rangle$	$\Sigma_{[\text{O II}]}$ ($\times 10^{38} \text{ erg s}^{-1} \text{ kpc}^{-2}$)	$\langle W_{2796} \rangle$ (Å)	$\langle z \rangle$	$\Sigma_{[\text{O II}]}$ ($\times 10^{38} \text{ erg s}^{-1} \text{ kpc}^{-2}$)
$1.0 \text{ \AA} \leq W_{2796} < 1.5 \text{ \AA}$	1.23	0.93	0.28 ± 0.04	1.23	0.89	0.37 ± 0.04
$1.5 \text{ \AA} \leq W_{2796} < 2.0 \text{ \AA}$	1.71	0.94	0.68 ± 0.06	1.73	0.90	0.49 ± 0.05
$2.0 \text{ \AA} \leq W_{2796} < 2.5 \text{ \AA}$	2.22	0.95	1.07 ± 0.09	2.23	0.91	0.99 ± 0.08
$3.0 \text{ \AA} \leq W_{2796} < 3.5 \text{ \AA}$	2.73	0.95	1.71 ± 0.13	2.72	0.92	1.36 ± 0.11
$3.5 \text{ \AA} \leq W_{2796} < 6.0 \text{ \AA}$	3.62	0.97	1.99 ± 0.15	3.66	0.91	1.33 ± 0.12

data are shown in *dot-dashed* line (i.e., $\langle \Sigma_{[\text{O II}]} \rangle = AW_0^\alpha$ with $\alpha = 1.28 \pm 0.11$ and $A = (2.95 \pm 0.29) \times 10^{37} \text{ erg s}^{-1} \text{ kpc}^{-2}$) in the figure. While this fit is not as good as that for DR7 data, what is evident is that the fit to DR12 data is consistently lower than that for the DR7 data in all but one equivalent width bin. This clearly confirms that the observed [O II] surface brightness is affected by fibre size effects even after normalizing the flux with the projected fibre size. In particular our results are consistent with the fact that (1) there is a large scatter in the W_{2796} vs impact parameter relationship even at high equivalent widths (see figure 1 of Nielsen et al. 2013; Lan et al. 2014; Huang et al. 2016) and (2) gradients are known to be present in the surface brightness profiles of galaxies which results in lower measured [O II] luminosities when smaller fibres probe predominately the outer parts of galaxies.

In the lower panel of Fig. 5 we also show the dependence of velocity width (deconvolved for the instrumental broadening) of [O II] line ($\sigma_{[\text{O II}]}$) on the W_{2796} of Mg II systems. A clear increasing trend of $\sigma_{[\text{O II}]}$ with W_{2796} is apparent from the figure. The $\sigma_{[\text{O II}]}$ increases from $\sim 90 \text{ km s}^{-1}$ to $\sim 200 \text{ km s}^{-1}$ when the average W_{2796} increases from 1 \AA to 3 \AA in both SDSS-DR7 and DR12. The [O II] line

profiles for each W_{2796} bin are shown in the upper panel of Fig. 5. One can see that emission line peaks for both the [O II] $\lambda\lambda 3727, 3729$ doublet components are clearly visible in the stacked profile of lower W_{2796} bins, i.e., $< 2.5 \text{ \AA}$. However, [O II] $\lambda\lambda 3727, 3729$ line is blended for the strong Mg II systems with $W_{2796} > 2.5 \text{ \AA}$. Typically σ of any emission line from a galaxy can be a good probe of the underlying mass. However, in the stacked spectrum it can also be a reflection of spread in the difference between emission and absorption redshifts. Therefore, a correlation between W_{2796} and $\sigma_{[\text{O II}]}$ could either reflect velocity offset (Δv) between emission and absorption increasing with W_{2796} and/or high W_{2796} systems originating from massive halos. However, in Paper 1 when we considered the direct [O II] detections we do not find any correlation between W_{2796} vs $\sigma_{[\text{O II}]}$ as well as W_{2796} vs Δv (relative velocity between absorption and emission redshift). It is also clear from Fig. 5, that $\sigma_{[\text{O II}]}$ measured for a given W_{2796} bin matches very well between SDSS-DR7 and SDSS-DR12. In addition, we do not find any dependence of [O II] $\lambda\lambda 3727, 3729$ doublet ratio with W_{2796} .

It is clear from the above discussions that $L_{[\text{O II}]}$ and $\Sigma_{[\text{O II}]}$ measured in the SDSS-DR12 composite are under estimated. Therefore, to minimize the fibre size effects, in

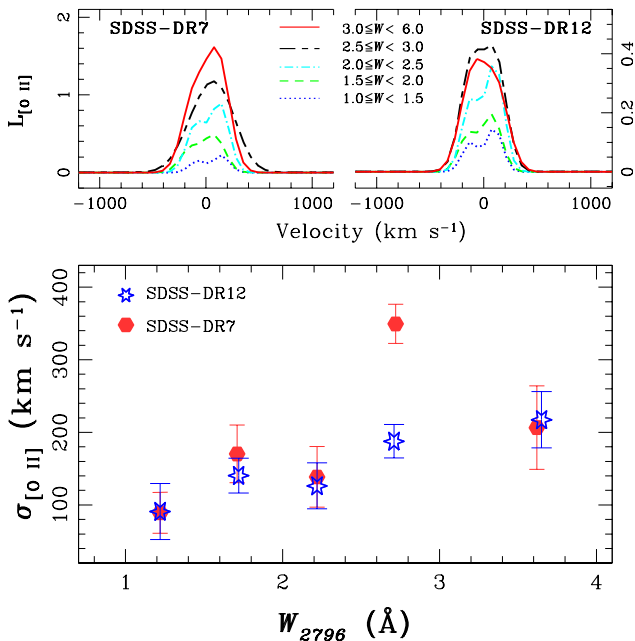


Figure 5. Lower panel: The distribution of $\sigma_{[\text{O II}]}$ as a function of W_{2796} for SDSS-DR7 (diamonds) and SDSS-DR12 (stars). Upper panel: shows the [O II] line profile for various W_{2796} bins for SDSS-DR7 and DR12.

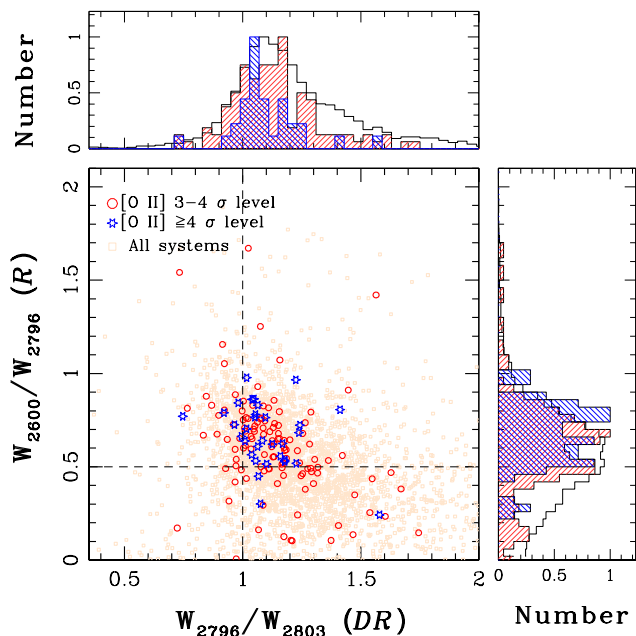


Figure 6. The Mg II doublet ratio versus \mathcal{R} parameter of Mg II absorbers with nebular emission line detected at $\geq 4\sigma$ (stars from Paper 1), $3-4\sigma$ (circles) and without (i.e., $< 3\sigma$) nebular emission (squares) line detection for $W_{2796} > 1 \text{ \AA}$ in SDSS-DR7. The upper and right-hand panels show, respectively, the DR and \mathcal{R} distributions for the Mg II systems with nebular emission line detected at $\geq 4\sigma$ (shaded with blue slanted lines at -45°), $3-4\sigma$ (shaded with red slanted lines at 45°) and without (i.e., $< 3\sigma$) nebular emission (unfilled histogram).

most discussions that follows we concentrate on results based on DR7.

4.2 Dependence of [O II] emission on $\mathcal{R} \equiv W_{2600}/W_{2796}$

In Paper 1, we have shown that for a given luminosity threshold (i.e. $L_{[\text{O II}]}$), direct [O II] nebular line detection fraction increases with increasing W_{2796} . We have considered [O II] detections with more than 4σ significance level in that study. Here, before doing the stacking analysis, we also identify systems with tentative emission feature (hereinafter, candidate [O II] emitters) at the expected position of [O II] at $3 < \sigma < 4$ level³. Note that by lowering the significance level to confirm a detection, we might have enhanced the number of false positives. In Fig. 6, we compare the distribution of these Mg II systems with (circles) and without (squares) emission feature in the \mathcal{R} vs DR plane (systems discussed in Paper 1 marked with star symbol). Interestingly, like the trend shown by firm detections, most of the Mg II systems with consistent features (at $3-4\sigma$ level) at the location of [O II] nebular line also have $\mathcal{R} \geq 0.5$ and $DR \sim 1$ (see also, figure 8 in Paper 1). In Fig. 6, we also plot the histogram of \mathcal{R} and DR distribution in the right and upper panel respectively. The sub-samples of “candidate [O II] emitters” and systems without nebular emission are found to be drawn from different distribution of \mathcal{R} with KS-test null probability of $p_{null} = 0.004$. It again indicates that the luminosity of [O II] emission in the stacked spectrum will depend on \mathcal{R} parameter.

To explore the dependence of average $L_{[\text{O II}]}$ and $\Sigma_{[\text{O II}]}$ emission on \mathcal{R} parameter we generate the composite spectra based on \mathcal{R} by dividing our sample into three bins of $\mathcal{R} \leq 0.44$, $0.44 < \mathcal{R} \leq 0.64$ and $\mathcal{R} > 0.64$, having almost equal number of systems in each bin. In Fig. 7, we show the median [O II] emission line profile in sub-samples based on \mathcal{R} parameter for SDSS-DR7. For comparison, we also show the stacked profiles from SDSS-DR12. It is apparent that the strength of [O II] emission is higher for the systems with higher \mathcal{R} parameter. This trend is consistent with the fact that when [O II] nebular emission is detected (with $\geq 3\sigma$ level of significance) in individual cases one finds \mathcal{R} values to be higher (see Fig. 6).

In order to decipher the effect of \mathcal{R} (without being affected by W_{2796} vs $L_{[\text{O II}]}$ correlations) on the strength of [O II] luminosity (or $\Sigma_{[\text{O II}]}$) we restrict ourselves to two narrow W_{2796} range of $1 \text{ \AA} \leq W_{2796} < 2 \text{ \AA}$ and $2 \text{ \AA} \leq W_{2796} < 3 \text{ \AA}$, having sufficient number of Mg II systems with $\mathcal{R} < 0.5$ (see Fig 2). Further, we divide each of them in to three bins of $\mathcal{R} \leq 0.44$, $0.44 < \mathcal{R} \leq 0.64$ and $\mathcal{R} > 0.64$. The details of these sub-samples are given in Table 2. The number of systems in each sub-sample, average W_{2796} and z_{abs} are given in column 2, 3 and 4 of this table, respectively. It is clear that these quantities do not differ by a wide margin between the sub-samples. However, we clearly see an increasing trend in $L_{[\text{O II}]}$ with \mathcal{R} .

A two-sided Kolmogorov-Smirnov test (KS test) shows that the W_{2796} distribution of two sub-samples with higher

³ Please refer to paper 1 for how we compute the significance level for the [O II] feature.

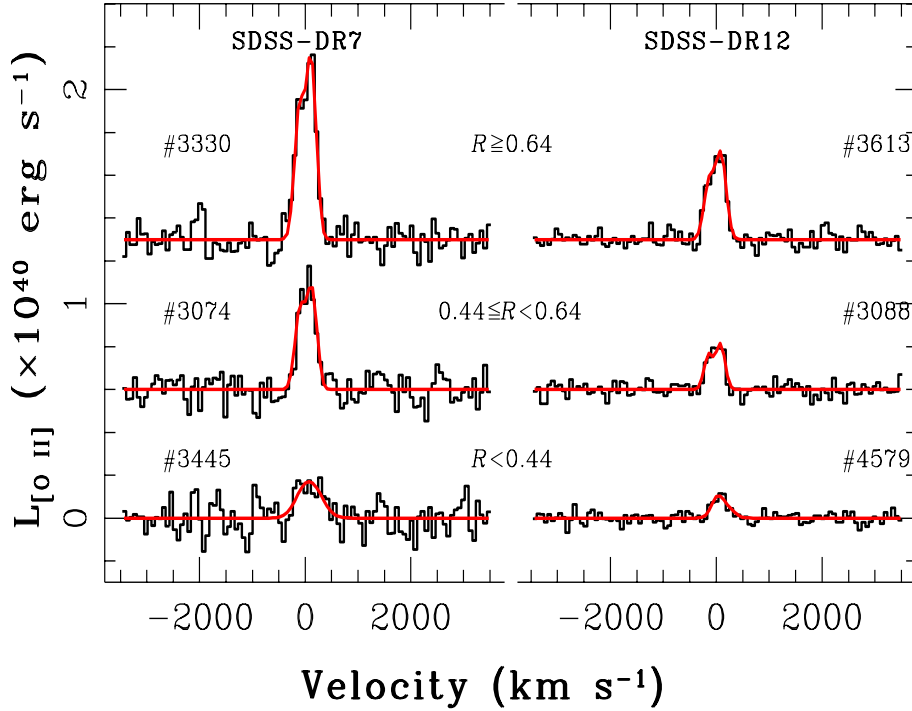


Figure 7. [O II] luminosity ($L_{[\text{O II}]}$) in the stacked spectra obtained for three bins of $\mathcal{R} \equiv W_{2600}/W_{2796}$ for strong ($W_{2796} > 1 \text{ \AA}$) Mg II absorbers detected in SDSS-DR7 spectra. *Right panel:* The same for the Mg II absorber detected in SDSS-DR12 spectra. Total number of Mg II systems involved in each bin is also given in the figure.

Table 2. The $L_{[\text{O II}]}$ for the subset based on \mathcal{R} parameter.

Criteria	No	$\langle W_{2796} \rangle$ (\AA)	$\langle z \rangle$	SDSS-DR7	
				$L_{[\text{O II}]}$ ($\times 10^{40} \text{ erg s}^{-1}$)	$L_{[\text{O II}]}^{P^a}$ ($\times 10^{40} \text{ erg s}^{-1}$)
1 $\text{\AA} \leq W_{2796} < 2 \text{ \AA}$					
$\mathcal{R} \leq 0.44$	2871	1.36	0.95	0.99 ± 0.26	1.66
$0.44 < \mathcal{R} \leq 0.64$	2169	1.42	0.93	1.48 ± 0.28	1.79
$\mathcal{R} > 0.64$	2291	1.43	0.92	2.76 ± 0.26	1.82
2 $\text{\AA} \leq W_{2796} < 3 \text{ \AA}$					
$\mathcal{R} \leq 0.44$	450	2.35	0.95	1.52 ± 0.69	4.40
$0.44 < \mathcal{R} \leq 0.64$	675	2.41	0.95	4.29 ± 0.59	4.60
$\mathcal{R} > 0.64$	801	2.41	0.94	7.94 ± 0.48	4.60

^a expected [O II] luminosity measured from the W_{2796} vs $L_{[\text{O II}]}$ correlation for the average W_{2796} per bin.

\mathcal{R} values, i.e., $0.44 < \mathcal{R} \leq 0.64$ and $\mathcal{R} > 0.64$, are drawn from a parent distribution with a null probability of being drawn from same parent distribution of $P_{KS} = 0.79$ and $P_{KS} = 0.87$ for both W_{2796} bins. The systems with $\mathcal{R} \leq 0.44$ show slightly lower W_{2796} . The average W_{2796} is lower by 4% in this case (i.e., $\mathcal{R} \leq 0.44$) compare to other two cases. We find that the probability for sub-samples with $\mathcal{R} \leq 0.44$ and $\mathcal{R} > 0.64$ are drawn from two different populations is $P_{KS} = 1.7 \times 10^{-11}$ (respectively, 0.03) for the systems having $1 \text{ \AA} \leq W_{2796} < 2 \text{ \AA}$ (respectively, $2 \text{ \AA} \leq W_{2796} < 3 \text{ \AA}$).

Next, we ask whether difference in $L_{[\text{O II}]}$ between $\mathcal{R} \leq 0.44$ and $\mathcal{R} > 0.64$ comes from the previously discussed correlation between W_{2796} and $L_{[\text{O II}]}$. Based on our $L_{[\text{O II}]}$ vs W_{2796} best fit parameters (i.e., AW_0^α with $\alpha = 0.97 \pm 0.07$ and $A = (1.78 \pm 0.08) \times 10^{40} \text{ erg s}^{-1}$) we compute the expected $L_{[\text{O II}]}$ for the mean W_{2796} probed by the above sub-samples and is given in column 6 of Table 2. It is clear

from this table that purely based on the W_{2796} vs $L_{[\text{O II}]}$ we do not expect $L_{[\text{O II}]}$ to be very different between different sub-samples. Interestingly, for a fixed W_{2796} range of $1 \text{ \AA} \leq W_{2796} < 2 \text{ \AA}$ a clear difference in $L_{[\text{O II}]}$ of factor 2.8 (significant at 3.6σ) is apparent for the subset having different \mathcal{R} parameter of $\mathcal{R} \leq 0.44$ and $\mathcal{R} > 0.64$. The difference in $L_{[\text{O II}]}$ is found to be even higher of about factor 5.7 (significant at 4.8σ) if we consider the systems with $2 \text{ \AA} \leq W_{2796} < 3 \text{ \AA}$.

The discussions presented here confirm that $L_{[\text{O II}]}$ obtained in the stacked spectra depends strongly on \mathcal{R} parameter.

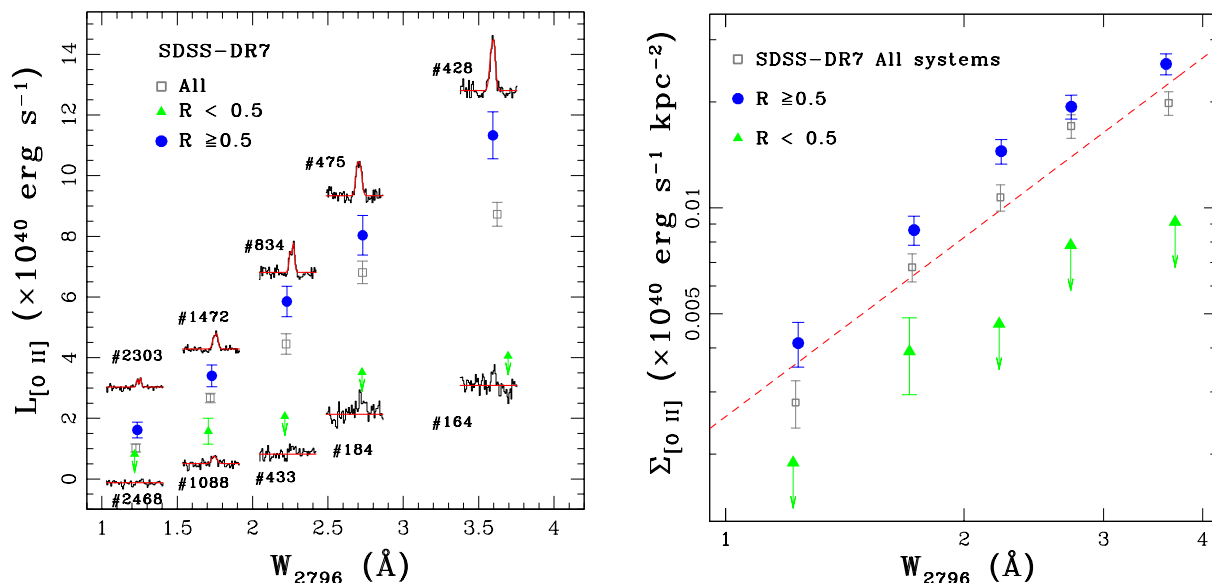


Figure 8. *Left panel:* The [O II] luminosity of Mg II systems detected in SDSS-DR7 with $R \geq 0.5$ (circles) and $R < 0.5$ (triangles) for various W_{2796} bins. The number of systems used for the stack and the stacked profiles are shown. The $L_{[\text{O II}]}$ for all the systems for different W_{2796} bins are shown as squares. *Right panel:* The [O II] luminosity surface density ($\Sigma_{[\text{O II}]}$) as a function of W_{2796} . The symbols are as in left panel. (circles).

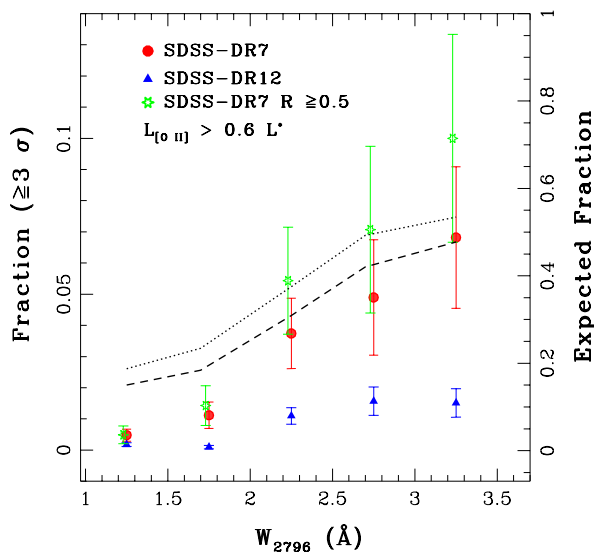


Figure 9. The fraction of Mg II systems with [O II] nebular emission detected at $\geq 3\sigma$ in SDSS-DR7 (circles) and DR12 (triangles). The dotted and dashed lines show the expected fraction of Mg II systems detected within a projected fibre radius of 10 and 7 kpc at a redshift of 0.6, from W_{2796} vs ρ distribution of confirmed Mg II galaxies by Nielsen et al. (2013), given in the right side ordinates.

4.3 Dependence of $L_{[\text{O II}]}$ versus W_{2796} based on \mathcal{R}

In this section we explore the effect of \mathcal{R} on $L_{[\text{O II}]}$ vs W_{2796} relation using SDSS-DR7 data. For this, we generate composite spectra for two subsets with $\mathcal{R} \geq 0.5$ and $\mathcal{R} < 0.5$ for various W_{2796} bins. In the left panel Fig. 8, we plot the $L_{[\text{O II}]}$

vs W_{2796} . We also show the [O II] profile for each W_{2796} bin for two ranges in \mathcal{R} . It is clear from the figure that the [O II] emission has systematically higher luminosity in the case of $\mathcal{R} \geq 0.5$ in each W_{2796} bin which is consistent with our findings discussed above. For the subset with $\mathcal{R} < 0.5$ we note that even for the lower W_{2796} bins, where there are a good number of systems available for the stacking, either the emission is significantly weaker or is not detected.

In right panel of Fig. 8, we show that the median surface luminosity density for the systems with $\mathcal{R} \geq 0.5$ (open circles) is higher than those of all Mg II systems (solid circles). It is clear from this figure that the correlation, we as well Ménard et al. (2011), found between $L_{[\text{O II}]}$ and W_{2796} in the whole Mg II sample is mainly dominated by systems showing strong Fe II. For systems with $\mathcal{R} < 0.5$ no clear trend between W_{2796} and $L_{[\text{O II}]}$ is visible and we could measure only upper limits in several W_{2796} bins.

Note, contrary to the correlation seen between W_{2796} and $L_{[\text{O II}]}$ (or $\Sigma_{[\text{O II}]}$) in the stacked spectra individual detections do not follow this correlation. In Paper 1, we suggested that the W_{2796} vs $L_{[\text{O II}]}$ correlation may come from increase in [O II] detection fraction with increasing W_{2796} . We explore this point further here.

In Fig. 9, we show the fraction of Mg II systems with an emission feature detected at $\geq 3\sigma$ at the expected location of [O II] doublet, having W_{2796} threshold of $\geq 1 \text{ \AA}$ and $L_{[\text{O II}]} \geq 0.6 L_{[\text{O II}]}^*$. A similar plot for Mg II systems with [O II] nebular emission detected at $\geq 4\sigma$ (~ 198 systems) are presented in Paper 1. Interestingly, we find a clear increasing trend between the fraction of Mg II systems with [O II] nebular emission and W_{2796} even among the tentative detections. A similar trend is also seen when we consider the fraction of systems with detection threshold of $\geq 2\sigma$ as well. This can be naturally explained with the known anti-

correlation between W_{2796} and ρ where the galaxies at lower projected distances (i.e., impact parameters) produce on an average stronger Mg II absorption and higher probability of the associated [O II] emission falling inside the fibre. The fraction further increases if we put an additional constraint of $\mathcal{R} \geq 0.5$. The reason being, as discussed in Fig. 6 most of the direct detections have $\mathcal{R} \geq 0.5$.

Using the impact parameter distribution of 183 spectroscopically confirmed Mg II galaxies from the compilation of Nielsen et al. (2013) we compute the detection fraction of Mg II systems within the impact parameter of ~ 10 and ~ 7 kpc for SDSS-DR7 and DR12, i.e., the projected radius of 3 and 2 arcsec fibres at $z = 0.6$. For this, we measure the average ρ and its standard deviation from the ρ distribution of Mg II systems for various W_{2796} bins. For each W_{2796} bin we compute the probability of galaxy to come inside the fibre by randomly generating 10,000 values of ρ by assuming a Gaussian distribution and considering 1σ error over each measurement. In Fig. 9, we show the expected fraction of Mg II systems in SDSS-DR7 (*dotted line*) and DR12 (*dashed line*) which roughly follow the observed trend in our systems. This once again reiterates the importance of anticorrelation between W_{2796} vs ρ and the fibre losses in deriving the correlations seen in the stacked spectra. However, it is important to note that the sample of Nielsen et al. (2013) does not contain enough systems at $\rho \leq 10$ kpc. As discussed before at such impact parameters the relationship between W_{2796} and ρ may not be similar to what we see at high ρ values. Thus it is very important to quantify the extent and nature of star forming regions associated with strong Mg II systems at low impact parameter through direct observations.

Our results also suggest that most of the Mg II absorbers with $\mathcal{R} \geq 0.5$ should have systematically lower impact parameter (or higher $L_{[\text{O II}]}$ and hence higher star formation rate) compared to those with $\mathcal{R} < 0.5$. We could not check this with the existing data of Nielsen et al. (2013) as Fe II $\lambda 2600$ measurements are not available for most of the systems.

4.4 Dependence of $L_{[\text{O II}]}$ versus z based on \mathcal{R}

The strong correlation between $\Sigma_{[\text{O II}]}$ and W_{2796} is also found to be evolving with redshift in the sense that a system with a given W_{2796} seems to be associated with larger $L_{[\text{O II}]}$ at high redshift compared to that at low redshift (Ménard et al. 2011). Such a redshift evolution of $L_{[\text{O II}]}$ is also seen among direct detections discussed in Paper 1. Here, to explore the dependence of $L_{[\text{O II}]}$ as a function of redshift based on \mathcal{R} parameter we make two subsets with W_{2796} bins of $1 \text{ \AA} \leq W_{2796} < 2 \text{ \AA}$ and $2 \text{ \AA} \leq W_{2796} < 6 \text{ \AA}$. We further divide each subset in to three redshift bins of $0.55 \leq z < 0.75$, $0.75 \leq z < 0.95$ and $0.95 \leq z < 1.3$, respectively. For these redshifts ranges, the fibre of 3 arcsec diameter used in SDSS-DR7 projects an angular size of 6.4 – 7.3 kpc, 7.3 – 7.9 kpc and 7.9 – 8.4 kpc, respectively, in the sky.

In Fig. 10, we show the $L_{[\text{O II}]}$ versus redshift as a function of \mathcal{R} for the subset with $1 \text{ \AA} \leq W_{2796} < 2 \text{ \AA}$ (*top left panel*) and $2 \text{ \AA} \leq W_{2796} < 6 \text{ \AA}$ (*top right panel*). It is clear from the figure that the median $L_{[\text{O II}]}$ of Mg II systems is higher at high redshifts. Here also, we note that the systems with $\mathcal{R} < 0.5$ show very less emission at each redshift bin, albeit having similar number of systems as in the sub-sample

Table 3. The best-fit parameters for the $\Sigma_{[\text{O II}]}$ as a function of redshift, $A(1+z)^\alpha$.

W_{2796} (\AA)	SDSS-DR7 with $\mathcal{R} \geq 0.5$	
	A	α
$1 \text{ \AA} \leq W_{2796} < 2 \text{ \AA}$	0.005 ± 0.003	0.01 ± 0.84
$2 \text{ \AA} \leq W_{2796} < 6 \text{ \AA}$	0.010 ± 0.002	0.98 ± 0.39

of $\mathcal{R} \geq 0.5$. The average $L_{[\text{O II}]}$ probed in the stacked spectra corresponds to sub- $L_{[\text{O II}]}$ [with $\log L_{[\text{O II}]}^* (\text{erg s}^{-1}) = 41.60$ at the median z of 0.65] galaxies with [O II] luminosity of $\sim 0.01 L_{[\text{O II}]}$ and $\sim 0.1 L_{[\text{O II}]}$, for the systems with W_{2796} ranging from $1 \text{ \AA} \leq W_{2796} < 2 \text{ \AA}$ and $2 \text{ \AA} \leq W_{2796} < 6 \text{ \AA}$, respectively. The *dashed curve* in Fig. 10 shows the expected luminosity of 0.1 and 0.03 $L_{[\text{O II}]}$ galaxy as a function of redshift using the redshift evolution of field galaxies luminosity function by Comparat et al. (2016, see their Table 7). Note that, these average luminosities are smaller than the direct detection of [O II] emission associated to individual Mg II systems (see figure 9, 10 of Paper 1). It is clear from Fig. 10 that the increase in $L_{[\text{O II}]}$ associated with Mg II systems roughly follows the luminosity evolution of field galaxies and is mostly due to the systems with $\mathcal{R} \geq 0.5$.

Next, to account for the effect of increasing fibre size with redshift we also plot $\Sigma_{[\text{O II}]}$ as a function of redshift for two equivalent width bins of $1 \text{ \AA} \leq W_{2796} < 2 \text{ \AA}$ (*lower left panel*) and $2 \text{ \AA} \leq W_{2796} < 6 \text{ \AA}$ (*lower right panel*). For $1 \text{ \AA} \leq W_{2796} < 2 \text{ \AA}$ the $\Sigma_{[\text{O II}]}$ seem to be constant with redshift. However, a mild increase in $\Sigma_{[\text{O II}]}$ with redshift is seen for the subset of $2 \text{ \AA} \leq W_{2796} < 6 \text{ \AA}$. We model $\Sigma_{[\text{O II}]}$ vs z with a power-law of the form $A(1+z)^\alpha$. The best fit parameters, i.e., normalization and slope for above two W_{2796} bins are given in column 2 and 3 of Table 3, respectively. We note that the evolution of $L_{[\text{O II}]}$ with redshift is similar (within 1σ) for both the subsets (see column 3 of Table 3).

Furthermore, we try to explore the contribution of direct detections to the stacked spectra. For this, we have selected systems with $1 \text{ \AA} \leq W_{2796} < 2 \text{ \AA}$ and $0.55 \leq z < 0.75$ where we have sufficient number of systems and the [O II] emission falls in the wavelength range free from most crowded telluric emission line region. Here, if one considers systems with $\mathcal{R} \geq 0.5$ where the [O II] emission is clearly detected, the $L_{[\text{O II}]}$ is found to be $(1.88 \pm 0.18) \times 10^{40}$ erg s $^{-1}$ (i.e., $\sim 0.047 L_{[\text{O II}]}$; where, $\log L_{[\text{O II}]}$ = 41.6 at average z of ~ 0.65). However, if we exclude the candidate [O II] emitters (i.e., systems with [O II] emission detected at $\geq 3\sigma$ level), which accounts for $\sim 5\%$ of the systems, we still detect the [O II] emission with slightly lower $L_{[\text{O II}]}$ of $(1.45 \pm 0.19) \times 10^{40}$ erg s $^{-1}$ (i.e., $0.036 L_{[\text{O II}]}$), albeit consistent within 1.6σ level. Here, it is interesting to ask that what kind of galaxies do contribute to this $L_{[\text{O II}]}$. For this, we first compute the average $L_{[\text{O II}]}$ of galaxies by using the [O II] luminosity function by Comparat et al. (2016) at average z of 0.65, for different lower limits on $L_{[\text{O II}]}$ ranging between $L_{\min} = 0.001 - 0.01 L_{[\text{O II}]}$, as:

$$\langle L \rangle = \frac{\int_{L_{\min}}^{L_{\max}} L \phi(L) dL}{\int_{L_{\min}}^{L_{\max}} \phi(L) dL}. \quad (1)$$

The average $L_{[\text{O II}]}$ expected for different values of L_{\min} are listed in column 2 of Table 4. It varies from $0.10 L_{[\text{O II}]}$ to $0.03 L_{[\text{O II}]}$ for the L_{\min} ranging from $0.01 L_{[\text{O II}]}$ and

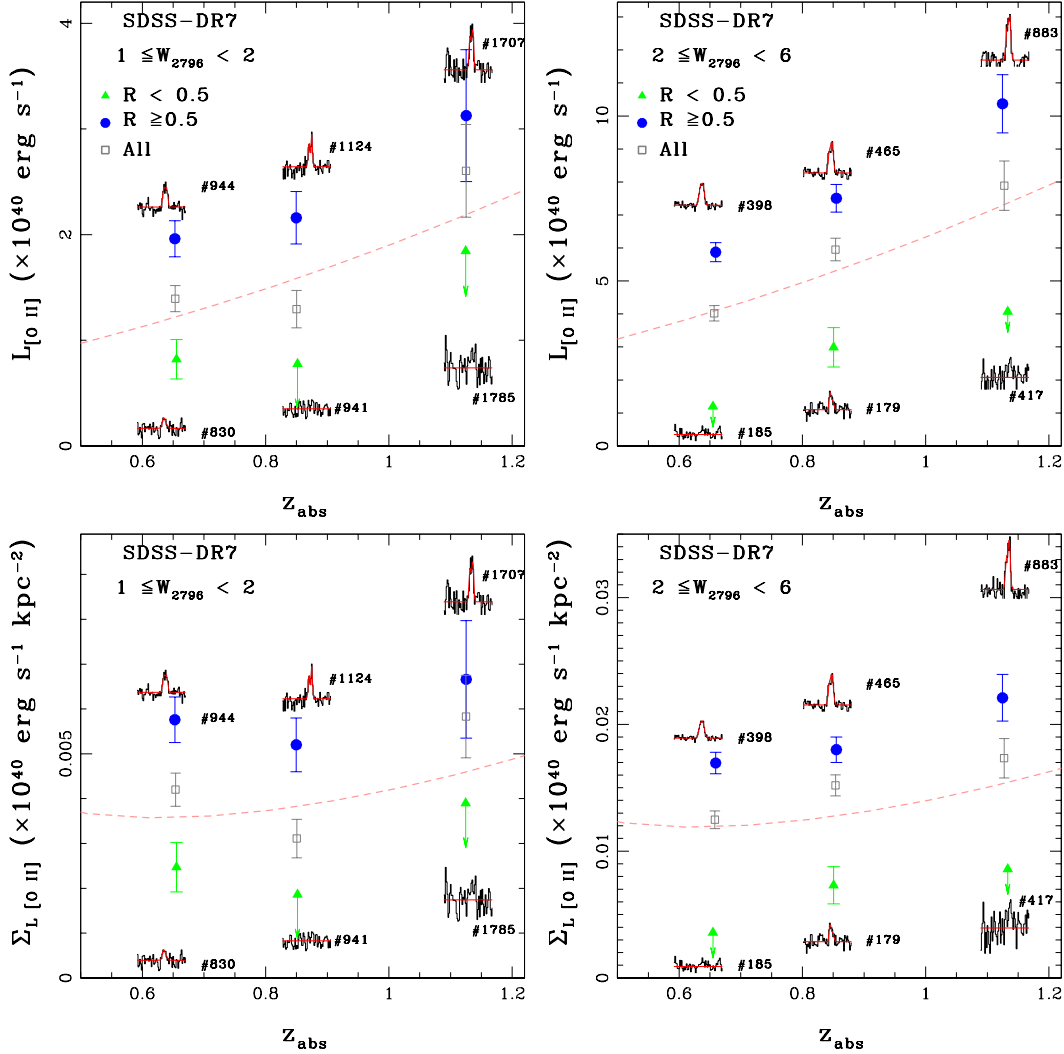


Figure 10. *Top left panel:* The [O II] luminosity as a function of z_{abs} for a subset of Mg II systems from SDSS-DR7 with $1 \text{ \AA} \leq W_{2796} < 2 \text{ \AA}$ and $R \geq 0.5$ (circles) and $R < 0.5$ (triangles), respectively. The $L_{[\text{O II}]}$ for all the systems is shown as squares. The number of systems used for the stack and the stacked profiles are shown. The dashed line show the luminosity evolution of $0.03L_{\star}$ (left panel) and $0.1L_{\star}$ (right panel) galaxy as a function of redshift. *Top right panel:* The same for the subset of Mg II systems with $2 \text{ \AA} \leq W_{2796} < 6 \text{ \AA}$. *Bottom panel:* show the $\Sigma_{[\text{O II}]}$ as a function of redshift for two W_{2796} bins of $1 \text{ \AA} \leq W_{2796} < 2 \text{ \AA}$ (left panel) and $2 \text{ \AA} \leq W_{2796} < 6 \text{ \AA}$ (right panel), respectively. The dashed line show the luminosity surface density evolution of $0.03L_{\star}$ (left panel) and $0.1L_{\star}$ (right panel) galaxy as a function of redshift.

$0.001 L_{[\text{O II}]}^{\star}$, respectively. Assuming that the average $L_{[\text{O II}]}$ detected in the stacked spectra after removal of candidate [O II] emitters is mainly due to galaxies with $L_{[\text{O II}]}$ smaller than that seen in case of direct detections, we compute the average $L_{[\text{O II}]}$ by restricting ourselves to $L_{\text{max}} = 0.23L_{[\text{O II}]}^{\star}$. This upper limit is set to the average luminosity of lower 5% systems from the cumulative distribution of [O II] luminosity of candidate [O II] emitters while considering it as the lowest $L_{[\text{O II}]}$ from direct detections. It is clear from Table 4, that we recover the observed $L_{[\text{O II}]}$ (i.e., $\sim 0.05L_{[\text{O II}]}^{\star}$) seen in the stacked spectra of all the Mg II systems when we integrate down to $0.003L_{[\text{O II}]}^{\star}$. Interestingly, the average $L_{[\text{O II}]}$ obtained by integrating the luminosity function over the luminosity range of $0.003L_{[\text{O II}]}^{\star}$ to $0.23L_{[\text{O II}]}^{\star}$ is similar to what we find in the stacked spectra without direct detections (i.e., $\sim 0.03L_{[\text{O II}]}^{\star}$). This clearly suggest that strong

Mg II absorbers also originate from low luminosity galaxies at small impact parameters. Note the above estimate is based on the assumption that galaxies are like point sources and without considering fibre losses. This should be considered more as an indicative result. The actual calculations should include size of galaxies, their orientations and fibre losses into account. We postpone this for a future work. In addition, the importance of low mass galaxies contributing to high W_{2796} absorbers can be probed through clustering analysis.

Therefore, based on the above discussions we conclude that within the impact parameters probed by the SDSS fibre(s) Mg II absorbers having higher R are associated with regions having higher $L_{[\text{O II}]}$. This means, either systems with high R originate from regions having high SFR (for a given impact parameter) or have smaller impact parameter

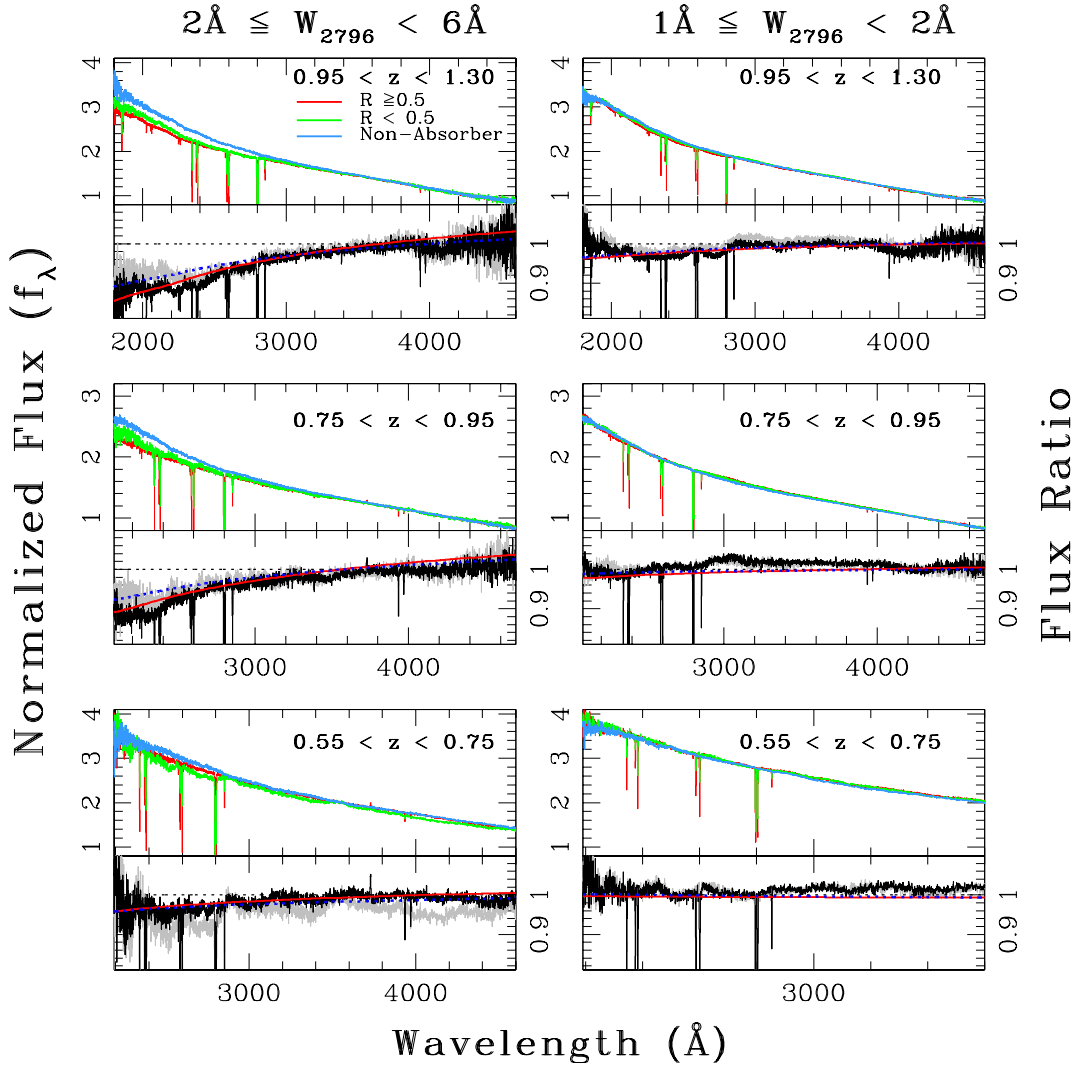


Figure 11. *Left panel:* The geometric mean composite spectra for the sub-samples with $2 \text{ \AA} \leq W_{2796} < 6 \text{ \AA}$ and three redshift bins of $0.55 \leq z < 0.75$ (bottom panel), $0.75 \leq z < 0.95$ (middle panel) and $0.95 \leq z < 1.30$ (top panel), respectively. The lower part of each panel shows the flux ratio of the two spectra for the systems with $\mathcal{R} \geq 0.5$ and control sample (black) along with the best fit SMC extinction curve (solid red line). The flux ratio for the systems with $\mathcal{R} < 0.5$ and control sample are shown in gray along with the best fit SMC extinction curve (dashed blue line). *Right panel:* The same as left for the subset with $1 \text{ \AA} \leq W_{2796} < 2 \text{ \AA}$.

Table 4. The average [O II] luminosity in the stacked spectra.

L_{\min}	Average $L_{[\text{O II}]}$ ^a	
($\times L_{[\text{O II}]}^*$)	$\langle L \rangle$	$\langle L^f \rangle = \frac{\int_{L_{\min}}^{0.23L^*} L \phi(L) dL}{\int_{L_{\min}}^{\infty} \phi(L) dL}$
0.01	0.10	0.042
0.005	0.07	0.031
0.003	0.05	0.024
0.001	0.03	0.015

^aThe upper limits is infinity for the second column and $0.23L_{[\text{O II}]}$ in the numerator for the third column.

ter to the star forming region (for a given W_{2796}). Obtaining spatially resolved spectroscopy as well as image stacking of these systems (Zibetti et al. 2007) could help in discriminating between these two alternatives.

4.5 Average dust content

Evidences for the presence of dust in the intervening absorbers are commonly seen in the form of continuum reddening. This makes quasar absorption systems to be a good tracers of dust content within gaseous haloes surrounding galaxies (York et al. 2006; Ménard et al. 2008; Khare et al. 2012; Ménard & Fukugita 2012; Fukugita & Ménard 2015; Sardane et al. 2015; Murphy & Bernet 2016). Here, we study the dependence of average dust content in Mg II systems on the \mathcal{R} parameter, i.e., $\mathcal{R} \geq 0.5$ and $\mathcal{R} < 0.5$. For this, we have made two subsets based on W_{2796} with $1 \text{ \AA} \leq W_{2796} < 2 \text{ \AA}$ and $2 \text{ \AA} \leq W_{2796} < 6 \text{ \AA}$. We further divide each subset into three redshift bins of $0.55 \leq z < 0.75$, $0.75 \leq z < 0.95$ and $0.95 \leq z < 1.30$. We have generated geometric mean spectra for various sub-samples as well as for the control samples of quasars, within $\Delta z = \pm 0.05$ of z_{em} and $\Delta r_{\text{mag}} = \pm 0.5$ of r_{mag} , without absorption in their spectra.

Table 5. The $E(B - V)$ for various sub-samples.

Redshift (z)	$E(B - V)$			
	$2 \text{ \AA} \leq W_{2796} < 6 \text{ \AA}$		$1 \text{ \AA} \leq W_{2796} < 2 \text{ \AA}$	
	$\mathcal{R} \geq 0.5$	$\mathcal{R} < 0.5$	$\mathcal{R} \geq 0.5$	$\mathcal{R} < 0.5$
$0.55 \leq z < 0.75$	0.011 ± 0.002	0.013 ± 0.004	-0.001 ± 0.002	-0.003 ± 0.001
$0.75 \leq z < 0.95$	0.027 ± 0.001	0.017 ± 0.004	0.004 ± 0.001	0.002 ± 0.001
$0.95 \leq z < 1.30$	0.026 ± 0.001	0.018 ± 0.002	0.005 ± 0.001	0.004 ± 0.001

The stacked spectra for various subsets are shown in Fig. 11. We estimate the reddening, $E(B - V)$, by fitting the spectral energy distribution (SED) of the control sample, reddened by the Small Magellanic Cloud (SMC) extinction curves (Gordon et al. 2003). The flux ratio of the composite spectra for the systems with $\mathcal{R} \geq 0.5$ (black) and $\mathcal{R} < 0.5$ (gray) to the control sample are shown in the lower panel of Fig. 11. The best fit SMC extinction curve for $\mathcal{R} \geq 0.5$ and $\mathcal{R} < 0.5$ sample are overlaid in *solid red* line and *dotted* line, respectively. We perform a bootstrap analysis to measure the uncertainties over each measurement. For this, we make stacked spectra for 1000 sub-samples by randomly selecting 70 per cent of the sample and measure the $E(B - V)$ by fitting the SED of control sample, reddened by SMC extinction curves. We consider the standard deviation of $E(B - V)$ distribution as 1σ uncertainty.

In Table 5, we have summarized the colour excess, $E(B - V)$, for each subset. At first, we confirm that the $E(B - V)$ is more towards high W_{2796} systems (Budzynski & Hewett 2011; Jiang et al. 2011) at any redshift bin. We also find that the $E(B - V)$ is higher for the systems at high redshift (see also, Budzynski & Hewett 2011; Ménard & Fukugita 2012). For the strong Mg II systems (i.e., $W_{2796} \geq 1\text{\AA}$) in our sample the $E(B - V)$ is found to be in the range of -0.001 to 0.027 . Using 809 Mg II absorption systems with $1.0 \leq z_{\text{abs}} \leq 1.86$ York et al. (2006) have shown that the typical colour excess, $E(B - V)$, introduced by these systems ranges from < 0.001 to 0.085 (see also, Wild et al. 2007). Interestingly, for the subset with $2 \text{ \AA} \leq W_{2796} < 6 \text{ \AA}$ and $0.95 \leq z < 1.3$ we find that Mg II systems with $\mathcal{R} \geq 0.5$ are redder (significant at 3.6σ level) than the systems with $\mathcal{R} < 0.5$. A similar trend is seen for the subset with $2 \text{ \AA} \leq W_{2796} < 6 \text{ \AA}$ and $0.75 \leq z < 0.95$ albeit with a lower significance at 2.4σ level. However, we do not see this trend for any other subsets (see also, Table 5). Note that the typical $E(B - V)$ of < 0.02 has been inferred using the DLAs (Vladilo et al. 2008) and ~ 0.046 from the Ca II absorbers with equivalent width of $\geq 0.7\text{\AA}$ (Sardane et al. 2015). Interestingly, the average $E(B - V)$ for the sub-sample with $2 \text{ \AA} \leq W_{2796} < 6 \text{ \AA}$ and redshift bins of $0.75 \leq z < 0.95$ and $0.95 \leq z < 1.3$ show the reddening of ~ 0.03 as seen in the extreme-DLAs, i.e., $\log N(\text{H I}) \geq 21.7$, by Noterdaeme et al. (2014). Moreover, the H I 21-cm absorbers that also show $\mathcal{R} \geq 0.5$ tend to produce more significant reddening in the spectrum of the background quasars than Mg II systems without 21-cm absorbers (Dutta et al. 2017).

5 DISCUSSION AND CONCLUSIONS

We have investigated the effect of fibre size as well as the metal absorption line ratio ($\mathcal{R} \equiv W_{2600}/W_{2796}$) on the average luminosity of [O II] $\lambda\lambda 3727, 3729$ nebular emission from Mg II absorbers (at $0.55 \leq z \leq 1.3$) in the composite spec-

tra by utilizing quasar spectra obtained with 3 and 2 arcsec fibres in Sloan Digital Sky Survey. We have found the following interesting results:

1. We confirm the presence of a strong correlation between [O II] luminosity and W_{2796} , in both the data sets. The $\Sigma_{[\text{O II}]}$ measured for SDSS-DR7 is found to be higher than those measured with SDSS-DR12. This suggests that the fibre effects are not fully taken care of even when we normalize the luminosity by the projected area. Interestingly, the difference is found to be largest for the highest W_{2796} bin of $3 - 6 \text{ \AA}$. This might be due to the observed large scatter between W_{2796} vs ρ relation which implies that even for the Ultra strong ($W_{2796} \geq 3 \text{ \AA}$) Mg II systems there is a non negligible probability of galaxy being outside the fibre (i.e., at large impact parameters). While discussing the difference between SDSS-DR7 and SDSS-DR12 observations we need to also remember some differences in the observational strategy adopted. In SDSS-DR7 the fibres are centered on red whereas in SDSS-DR12 a centering offset is introduced to the fibres, taking into account atmospheric dispersion, to improve the flux on blue part. At this stage it is not clear what is the contribution of this effect to the differences we discuss in this work. Therefore, it is important to systematically study a sample of strong Mg II systems with integral field spectroscopy to map the extent and nature of star formation associated with Mg II systems of different equivalent widths.

2. We also explore the dependence of $L_{[\text{O II}]}$ on $\mathcal{R} \equiv W_{2600}/W_{2796}$. We have found that the Mg II absorbers with $\mathcal{R} \geq 0.5$ tend to show higher $L_{[\text{O II}]}$ and $\Sigma_{[\text{O II}]}$ (see Fig. 8). In fact, the strong correlation seen between $L_{[\text{O II}]}$ vs W_{2796} and $L_{[\text{O II}]}$ vs z is mainly driven by systems with strong Fe II (i.e. $\mathcal{R} \geq 0.5$). For systems with $\mathcal{R} < 0.5$ no such trend between W_{2796} and $L_{[\text{O II}]}$ is visible. We also show that the fraction of systems with direct detection increases as a function of W_{2796} which gives a hint that the strong correlation seen in the stacked spectra is possibly a combined result of the W_{2796} versus ρ anti-correlation and the redshift dependent fibre losses.

3. Strong dependence of [O II] luminosity on \mathcal{R} could mean the correlation between impact parameter and \mathcal{R} could be stronger than that between W_{2796} and impact parameter. It will be important to check this before ascribing any physical connection between \mathcal{R} and star formation rate associated with the absorbing galaxy. Unfortunately \mathcal{R} values are not available for systems used to define the correlation between W_{2796} and ρ (Nielsen et al. 2013). Therefore, it will be an important step to explore the correlation between W_{2796} and \mathcal{R} for building a clear connection between W_{2796} and associated star formation rate.

4. We clearly detect the [O II] emission in the stacked spectra even if we exclude the candidate [O II] emitters (systems with nebular emission detected at $\geq 3\sigma$ level of significance). This could either means appreciable contribution

from low luminosity galaxies at small impact parameters or galaxies at larger impact parameters with only light from outer regions of galaxies contributing to the emission in the stacked spectra.

5. We confirm the trend of increasing $E(B - V)$ of Mg II absorbers with increasing W_{2796} as well as redshift (see also Fig. 11). Interestingly, for the subset with $2 \text{ \AA} \leq W_{2796} < 6 \text{ \AA}$ and $0.95 \leq z < 1.3$ the $E(B - V)$ of Mg II systems with $\mathcal{R} \geq 0.5$ is found to be higher than that for the systems with $\mathcal{R} < 0.5$ (at 3.6σ level). The $E(B - V)$ found in $\mathcal{R} > 0.5$ is similar to the $E(B - V)$ inferred for DLAs. Using the Mg II systems searched for the H I absorption in STIS survey by Rao et al. (2006) and Rao et al. (2017) we compute the fraction of strong Mg II systems ($W_{2796} \geq 1 \text{ \AA}$) having $\mathcal{R} \geq 0.5$ being DLAs, i.e., $\log N(\text{H I}) \geq 20.3$, is $\sim 38\%$ which is only $\sim 6\%$ in case of $\mathcal{R} < 0.5$. This fraction increase to $\sim 60\%$ if we consider the systems with $W_{2796} \geq 2 \text{ \AA}$ and $\mathcal{R} \geq 0.5$. Therefore, the Mg II absorbers with $\mathcal{R} \geq 0.5$ systems may be related to high probability of them being sub-DLA and DLAs.

ACKNOWLEDGMENTS

RS, PN, and PPJ acknowledge the support from Indo-French Centre for the Promotion of Advance Research (IFC-PAR) under project number 5504–2.

Funding for the Sloan Digital Sky Survey IV has been provided by the Alfred P. Sloan Foundation, the U.S. Department of Energy Office of Science, and the Participating Institutions. SDSS-IV acknowledges support and resources from the Center for High-Performance Computing at the University of Utah. The SDSS web site is www.sdss.org.

SDSS-IV is managed by the Astrophysical Research Consortium for the Participating Institutions of the SDSS Collaboration including the Brazilian Participation Group, the Carnegie Institution for Science, Carnegie Mellon University, the Chilean Participation Group, the French Participation Group, Harvard-Smithsonian Center for Astrophysics, Instituto de Astrofísica de Canarias, The Johns Hopkins University, Kavli Institute for the Physics and Mathematics of the Universe (IPMU) / University of Tokyo, Lawrence Berkeley National Laboratory, Leibniz Institut für Astrophysik Potsdam (AIP), Max-Planck-Institut für Astronomie (MPIA Heidelberg), Max-Planck-Institut für Astrophysik (MPA Garching), Max-Planck-Institut für Extraterrestrische Physik (MPE), National Astronomical Observatories of China, New Mexico State University, New York University, University of Notre Dame, Observatório Nacional / MCTI, The Ohio State University, Pennsylvania State University, Shanghai Astronomical Observatory, United Kingdom Participation Group, Universidad Nacional Autónoma de México, University of Arizona, University of Colorado Boulder, University of Oxford, University of Portsmouth, University of Utah, University of Virginia, University of Washington, University of Wisconsin, Vanderbilt University, and Yale University.

REFERENCES

- Bergeron J., 1986, *A&A*, **155**, L8
 Bolton A. S., et al., 2012, *AJ*, **144**, 144
 Bordoloi R., et al., 2011, *ApJ*, **743**, 10

- Bouché N., Hohensee W., Vargas R., Kacprzak G. G., Martin C. L., Cooke J., Churchill C. W., 2012, *MNRAS*, **426**, 801
 Budzynski J. M., Hewett P. C., 2011, *MNRAS*, **416**, 1871
 Chelouche D., Bowen D. V., 2010, *ApJ*, **722**, 1821
 Chen H.-W., Helsby J. E., Gauthier J.-R., Shectman S. A., Thompson I. B., Tinker J. L., 2010, *ApJ*, **714**, 1521
 Comparat J., et al., 2016, *MNRAS*, **461**, 1076
 Dey A., Torrey P., Rubin K. H. R., Zhu G. B., Suresh J., 2015, *MNRAS*, **451**, 1806
 Dutta R., Srianand R., Gupta N., Joshi R., Petitjean P., Noterdaeme P., Ge J., Krogager J.-K., 2017, *MNRAS*, **465**, 4249
 Erb D. K., 2008, *ApJ*, **674**, 151
 Fukugita M., Ménard B., 2015, *ApJ*, **799**, 195
 Gordon K. D., Clayton G. C., Misselt K. A., Landolt A. U., Wolff M. J., 2003, *ApJ*, **594**, 279
 Gupta N., Srianand R., Petitjean P., Bergeron J., Noterdaeme P., Muzahid S., 2012, *A&A*, **544**, A21
 Heckman T. M., 2001, in Hibbard J. E., Rupen M., van Gorkom J. H., eds, *Astronomical Society of the Pacific Conference Series Vol. 240, Gas and Galaxy Evolution*. p. 345 ([arXiv:astro-ph/0009075](https://arxiv.org/abs/astro-ph/0009075))
 Heckman T. M., 2002, in Mulchaey J. S., Stocke J. T., eds, *Astronomical Society of the Pacific Conference Series Vol. 254, Extragalactic Gas at Low Redshift*. p. 292 ([arXiv:astro-ph/0107438](https://arxiv.org/abs/astro-ph/0107438))
 Huang Y.-H., Chen H.-W., Johnson S. D., Weiner B. J., 2016, *MNRAS*, **455**, 1713
 Jiang P., Ge J., Zhou H., Wang J., Wang T., 2011, *ApJ*, **732**, 110
 Joshi R., Srianand R., Noterdaeme P., Petitjean P., 2017a, *MNRAS*, **465**, 701
 Joshi R., Srianand R., Petitjean P., Noterdaeme P., 2017b, *MNRAS*, **471**, 1910
 Kacprzak G. G., Churchill C. W., Nielsen N. M., 2012, *ApJ*, **760**, L7
 Khare P., vanden Berk D., York D. G., Lundgren B., Kulkarni V. P., 2012, *MNRAS*, **419**, 1028
 Lan T.-W., Ménard B., Zhu G., 2014, *ApJ*, **795**, 31
 Lanzetta K. M., Bowen D. V., 1992, *ApJ*, **391**, 48
 López G., Chen H.-W., 2012, *MNRAS*, **419**, 3553
 Lundgren B. F., et al., 2012, *ApJ*, **760**, 49
 Martin C. L., Shapley A. E., Coil A. L., Kornei K. A., Bundy K., Weiner B. J., Noeske K. G., Schiminovich D., 2012, *ApJ*, **760**, 127
 Ménard B., Fukugita M., 2012, *ApJ*, **754**, 116
 Ménard B., Nestor D., Turnshek D., Quider A., Richards G., Chelouche D., Rao S., 2008, *MNRAS*, **385**, 1053
 Ménard B., Wild V., Nestor D., Quider A., Zibetti S., Rao S., Turnshek D., 2011, *MNRAS*, **417**, 801
 Mo H. J., Miralda-Escude J., 1996, *ApJ*, **469**, 589
 Murphy M. T., Bernet M. L., 2016, *MNRAS*, **455**, 1043
 Nestor D. B., Johnson B. D., Wild V., Ménard B., Turnshek D. A., Rao S., Pettini M., 2011, *MNRAS*, **412**, 1559
 Newman S. F., et al., 2012, *ApJ*, **761**, 43
 Nielsen N. M., Churchill C. W., Kacprzak G. G., Murphy M. T., 2013, *ApJ*, **776**, 114
 Nielsen N. M., Churchill C. W., Kacprzak G. G., Murphy M. T., Evans J. L., 2016, *ApJ*, **818**, 171
 Noterdaeme P., Srianand R., Mohan V., 2010, *MNRAS*, **403**, 906
 Noterdaeme P., Petitjean P., Pâris I., Cai Z., Finley H., Ge J., Pieri M. M., York D. G., 2014, *A&A*, **566**, A24
 Osterbrock D. E., Ferland G. J., 2006, *Astrophysics of gaseous nebulae and active galactic nuclei*
 Pettini M., Shapley A. E., Steidel C. C., Cuby J.-G., Dickinson M., Moorwood A. F. M., Adelberger K. L., Gialalisco M., 2001, *ApJ*, **554**, 981
 Rahmani H., Srianand R., Noterdaeme P., Petitjean P., 2010, *MNRAS*, **409**, L59
 Rao S. M., Turnshek D. A., Nestor D. B., 2006, *ApJ*, **636**, 610

Rao S. M., Turnshek D. A., Sardane G. M., Monier E. M., 2017, *MNRAS*, **471**, 3428
 Sardane G. M., Turnshek D. A., Rao S. M., 2015, *MNRAS*, **452**, 3192
 Schaye J., 2001, *ApJ*, **559**, L1
 Seko A., Ohta K., Yabe K., Hatsukade B., Akiyama M., Tamura N., Iwamuro F., Dalton G., 2016, *ApJ*, **833**, 53
 Shapley A. E., Steidel C. C., Pettini M., Adelberger K. L., 2003, *ApJ*, **588**, 65
 Simcoe R. A., Sullivan P. W., Cooksey K. L., Kao M. M., Matejek M. S., Burgasser A. J., 2012, *Nature*, **492**, 79
 Srianand R., 1996, *ApJ*, **462**, 643
 Srianand R., Petitjean P., Ledoux C., Ferland G., Shaw G., 2005, *MNRAS*, **362**, 549
 Steidel C. C., 1995, in Meylan G., ed., QSO Absorption Lines. p. 139 ([arXiv:astro-ph/9509098](https://arxiv.org/abs/astro-ph/9509098))
 Steidel C. C., Erb D. K., Shapley A. E., Pettini M., Reddy N., Bogosavljević M., Rudie G. C., Rakic O., 2010, *ApJ*, **717**, 289
 Tinker J. L., Chen H.-W., 2008, *ApJ*, **679**, 1218
 Vladilo G., Prochaska J. X., Wolfe A. M., 2008, *A&A*, **478**, 701
 Weisheit J. C., 1978, *ApJ*, **219**, 829
 Wild V., Hewett P. C., Pettini M., 2007, *MNRAS*, **374**, 292
 Wolfe A. M., Gawiser E., Prochaska J. X., 2003, *ApJ*, **593**, 235
 York D. G., et al., 2006, *MNRAS*, **367**, 945
 Zhu G., Ménard B., 2013, *ApJ*, **770**, 130
 Zhu G. B., et al., 2015, *ApJ*, **815**, 48
 Zibetti S., Ménard B., Nestor D. B., Quider A. M., Rao S. M., Turnshek D. A., 2007, *ApJ*, **658**, 161

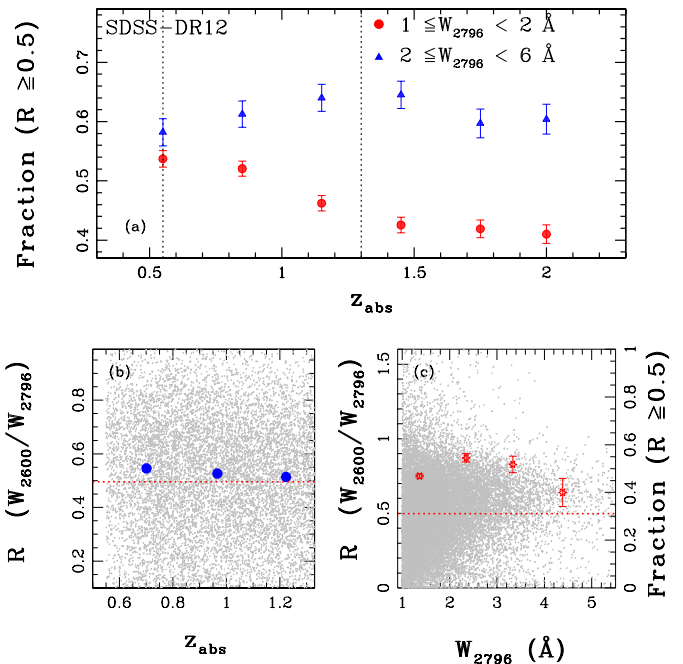


Figure A1. Same as Fig. 2 for Mg II systems from SDSS-DR12.

APPENDIX A:

A1 Properties of SDSS-DR12 Mg II systems:

In Fig. A1, we show the fraction of Mg II systems with $R \geq 0.5$ as a function of redshift versus z for two different W_{2796} ranges for SDSS-DR12 dataset. We see the similar trend of \mathcal{R} as a function of redshift and equivalent width for the Mg II systems detected in SDSS-DR7 data-set.

A2 Average [O II] emission: Dependence on continuum fit:

Here, we show that the significant difference in the $\Sigma_{[\text{O II}]}$ between our measurement with Ménard et al. (2011), as shown in Fig. 4, is mainly due to the difference in the modelled continuum. In the upper panel of Fig. A2, we show the continuum fits for SDSSJ010226.76+140740.5 modelled by a low order (typically a third order) polynomial (*dashed line*) and also modelled by an iterative running median of sizes ranging from 500 to 15 pixels (*solid line*) as used by Ménard et al. (2011). It is apparent from figure that the running median continuum smooths all the small scale fluctuation and resulting in smaller [O II] emission. In the lower panel of Fig. A2, we compare the $\Sigma_{[\text{O II}]}$ as a function W_{2796} from the above two methods of continuum modelling. The $\Sigma_{[\text{O II}]}$ measured from the stacked spectra generated using a local continuum (*circle*) is higher than the one obtained from running median (*stars*). It is clear from the figure that the $\Sigma_{[\text{O II}]}$ measurement from the continuum fit procedure of Ménard et al. (2011) are consistent with their best fit model.

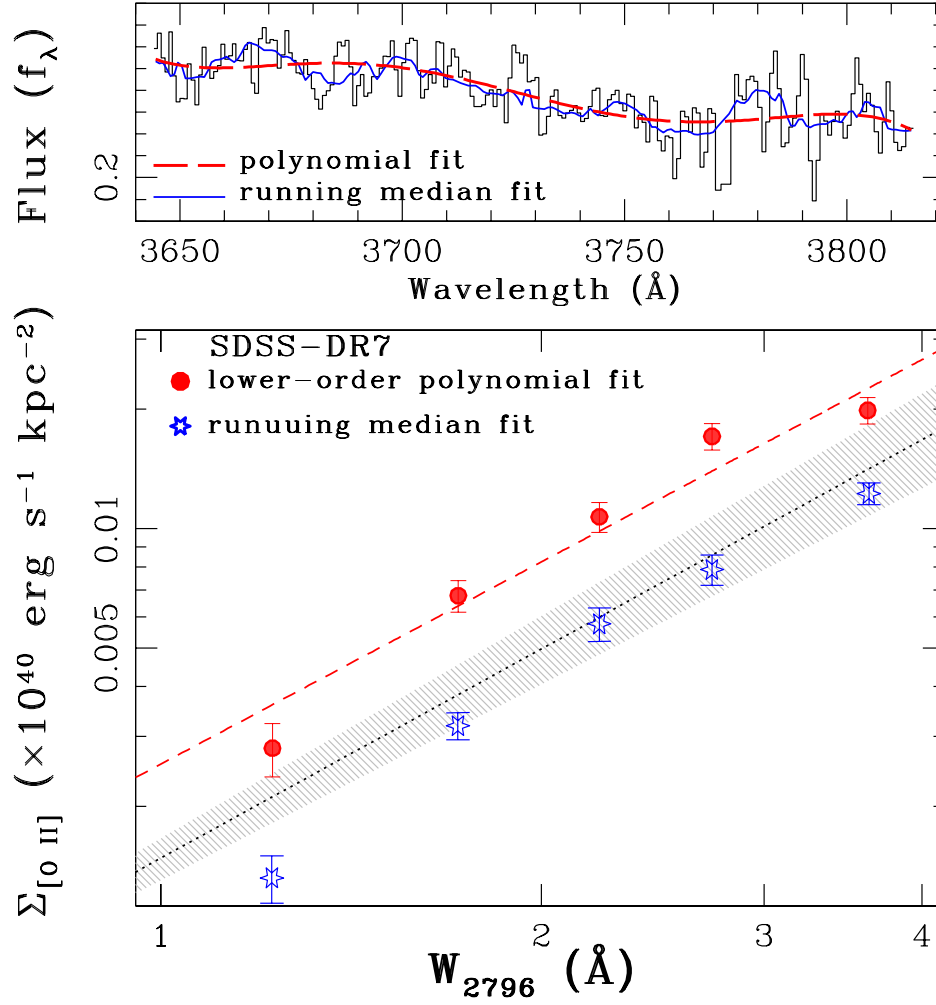


Figure A2. *Lower panel:* The [O II] luminosity surface density ($\Sigma_{[\text{O II}]}$) as a function of W_{2796} for SDSS-DR7 for the stacked spectra with continuum modelled as lower order polynomial (*red circles*) and the continuum modelled as iterative running median of sizes ranging from 500 to 15 pixels (*blue stars*). *Upper panel:* The spectral chunk around [O II] nebular emission along with the modelled continuum fit using a low order polynomial (*dashed line*). The continuum fit for entire spectra using iterative running median of sizes ranging from 500 to 15 pixels is shown in *solid line*.